Initial-value problem for three-dimensional disturbances in a compressible boundary layer

Eric Forgoston and Anatoli Tumin[a)]
The University of Arizona, Tucson, Arizona 85721

(Received 19 August 2004; accepted 8 July 2005; published online 23 August 2005)

An initial-value problem is formulated for a three-dimensional wave packet in a compressible boundary layer flow. The problem is solved using a Laplace transform with respect to time and Fourier transforms with respect to the streamwise and spanwise coordinates. The solution can be presented as a sum of modes consisting of continuous and discrete spectra of temporal stability theory. Two discrete modes, known as mode S and mode F, are of interest in high-speed flows since they may be involved in a laminar-turbulent transition scenario. The continuous and discrete spectrum are analyzed numerically for a hypersonic flow with Mach number $M=5.6$. The following features are revealed: (1) The synchronism of mode S with acoustic waves at a streamwise wave number $\alpha \to 0$ is primarily two-dimensional; (2) at high angles of disturbance propagation, mode F is no longer synchronized with entropy and vorticity waves; (3) at high angles of disturbance propagation, the synchronism between mode S and mode F is not accompanied by a mode S instability, and at even higher angles of disturbance propagation, mode S and mode F are not synchronized. © *2005 American Institute of Physics*. [DOI: 10.1063/1.2013261]

I. INTRODUCTION

The transition process from laminar to turbulent flow in hypersonic boundary layers has been studied for many years. However, our understanding of this phenomenon is still very poor compared to the low-speed case.[1] Several reasons exist for this difference. For example, experimental conditions are severe in hypersonic wind tunnels. Because of high levels of free-stream noise, it is difficult to perform experiments with controlled disturbances. Unlike the low-speed case,[2] it is difficult to design perturbers that can generate high-frequency artificial disturbances of individual modes. Instead, wave trains and wave packets are generated. Therefore, interpretation of experimental data is not straightforward, and this issue leads to the need for close coordination between theoretical modeling and experimental design and testing.[3]

Experiments with controlled disturbances could provide insight into the governing mechanisms associated with hypersonic laminar-turbulent transition, with a sharp cone being a good candidate for transition studies due to its relatively simple geometry. Several methods for excitation of artificial disturbances in a hypersonic boundary layer are available. These methods could be used to generate either two-dimensional (2D) or three-dimensional (3D) wave packets of a broad frequency band.

Additionally, due to advances in computational fluid dynamics, it is possible to perform reliable simulations of laminar-turbulent transition. Ma and Zhong[4,5] and Zhong and Ma[6] have performed direct numerical simulations to better understand the mechanisms leading to hypersonic boundary layer transition.

Accompanying these experiments, both wind tunnel and numerical, should be theoretical modeling and studies of the development of wave packets in hypersonic boundary layers.

Gustavsson[7] solved a 2D initial-value problem for incompressible boundary layer flows. Fedorov and Tumin[3] analyzed a 2D initial-value problem in a compressible boundary layer. However, the problem for 3D wave packets has not yet been considered.

Mack[8,9] used linear stability theory to perform extensive studies of the behavior of 2D and 3D instability modes for both the temporal and spatial problems. In particular, he discovered that for compressible flows, higher acoustic instability modes exist along with the first mode. However, even though the behavior of these modes is understood, the mechanism by which the modes are generated (receptivity problem) is still a subject of research. Throughout the 1980's, 1990's, and 2000's, Fedorov and colleagues discovered many results involving the receptivity of high-speed flows. One can find a complete bibliography in Ref. 10.

Particularly, this spatial analysis of the 2D instability modes in hypersonic flows revealed the following: (1) in the region of the leading edge, two discrete modes, mode F and mode S (we use Fedorov's[10] terminology), are synchronized with fast and slow acoustic waves, respectively; (2) at a downstream location, mode F is synchronized with the entropy and vorticity waves; (3) further downstream, mode F and mode S could also become synchronized.[11] It is important to understand these features due to the role they may have in the transition process. Later on, similar features of mode F and mode S were seen in the 2D temporal problem.[3]

Our objective is to solve the initial-value problem for a 3D wave packet in a compressible boundary layer flow. Additionally, we will use a numerical example to illustrate features of the spectrum that are associated with the 3D character of the problem.

[a)]Author to whom correspondence should be addressed. Electronic mail: tumin@engr.arizona.edu

II. PROBLEM FORMULATION

We consider a 3D parallel boundary layer flow of a calorically perfect gas. At the initial time, $t=0$, a 3D localized disturbance is introduced into the flow. The problem is to describe the downstream evolution of the perturbation. The hydrodynamic and thermodynamic characteristics of the flow are expressed as a superposition $Q_s(y)+q(x,y,z,t)$, where Q_s is a mean-flow quantity and q is its disturbance. The streamwise, normal, and spanwise spatial coordinates, given respectively by x, y, z, are nondimensionalized using a length scale L^*, and time is nondimensionalized as L^*/U_e^*, where U_e^* is the streamwise mean velocity at the upper boundary layer edge. The mean-flow velocity components are referenced to U_e^*, while temperature, density, and viscosity are referenced to their respective quantities at the upper boundary layer edge. Pressure is made nondimensional, using the dynamic pressure, $\rho_e^*(U_e^*)^2$. We denote u, v, and w to be respectively the streamwise, normal, and spanwise velocity disturbances, and θ, π, ρ, and μ to be respectively the temperature, pressure, density, and viscosity disturbances. The linearized, dimensionless, governing equations for the disturbances are

$$\frac{\partial \rho}{\partial t}+\rho_s\frac{\partial u}{\partial x}+U_s\frac{\partial \rho}{\partial x}+\frac{\partial}{\partial y}(\rho_s v)+\rho_s\frac{\partial w}{\partial z}+W_s\frac{\partial \rho}{\partial z}=0, \tag{1a}$$

$$\begin{aligned}\rho_s\left(\frac{\partial u}{\partial t}+U_s\frac{\partial u}{\partial x}+v\frac{\partial U_s}{\partial y}+W_s\frac{\partial u}{\partial z}\right)&=-\frac{\partial \pi}{\partial x}+\frac{1}{\mathrm{Re}}\left\{\frac{\partial}{\partial x}\left[\mu_s\left(r\frac{\partial u}{\partial x}+m\frac{\partial v}{\partial y}+m\frac{\partial w}{\partial z}\right)\right]\right.\\&+\frac{\partial}{\partial y}\left[\mu_s\left(\frac{\partial u}{\partial y}+\frac{\partial v}{\partial x}\right)+\mu\left(\frac{\partial U_s}{\partial y}\right)\right]\\&\left.+\frac{\partial}{\partial z}\left[\mu_s\left(\frac{\partial w}{\partial x}+\frac{\partial u}{\partial z}\right)\right]\right\},\end{aligned} \tag{1b}$$

$$\begin{aligned}\rho_s\left(\frac{\partial v}{\partial t}+U_s\frac{\partial v}{\partial x}+W_s\frac{\partial v}{\partial z}\right)&=-\frac{\partial \pi}{\partial y}+\frac{1}{\mathrm{Re}}\left\{\frac{\partial}{\partial x}\left[\mu_s\left(\frac{\partial u}{\partial y}+\frac{\partial v}{\partial x}\right)+\mu\left(\frac{\partial U_s}{\partial y}\right)\right]\right.\\&+\frac{\partial}{\partial y}\left[\mu_s\left(m\frac{\partial u}{\partial x}+r\frac{\partial v}{\partial y}+m\frac{\partial w}{\partial z}\right)\right]\\&\left.+\frac{\partial}{\partial z}\left[\mu_s\left(\frac{\partial v}{\partial z}+\frac{\partial w}{\partial y}\right)+\mu\left(\frac{\partial W_s}{\partial y}\right)\right]\right\},\end{aligned} \tag{1c}$$

$$\begin{aligned}\rho_s\left(\frac{\partial w}{\partial t}+U_s\frac{\partial w}{\partial x}+v\frac{\partial W_s}{\partial y}+W_s\frac{\partial w}{\partial z}\right)&=-\frac{\partial \pi}{\partial z}+\frac{1}{\mathrm{Re}}\left\{\frac{\partial}{\partial x}\left[\mu_s\left(\frac{\partial w}{\partial x}+\frac{\partial u}{\partial z}\right)\right]\right.\\&+\frac{\partial}{\partial y}\left[\mu_s\left(\frac{\partial v}{\partial z}+\frac{\partial w}{\partial y}\right)+\mu\left(\frac{\partial W_s}{\partial y}\right)\right]\\&\left.+\frac{\partial}{\partial z}\left[\mu_s\left(m\frac{\partial u}{\partial x}+m\frac{\partial v}{\partial y}+r\frac{\partial w}{\partial z}\right)\right]\right\},\end{aligned} \tag{1d}$$

$$\begin{aligned}\rho_s\left(\frac{\partial \theta}{\partial t}+U_s\frac{\partial \theta}{\partial x}+v\frac{\partial T_s}{\partial y}+W_s\frac{\partial \theta}{\partial z}\right)&=(\gamma-1)M_e^2\left(\frac{\partial \pi}{\partial t}+U_s\frac{\partial \pi}{\partial x}+W_s\frac{\partial \pi}{\partial z}+\frac{1}{\mathrm{Re}}\Phi\right)\\&+\frac{1}{\mathrm{Re\,Pr}}\left[\frac{\partial}{\partial x}\left(\mu_s\frac{\partial \theta}{\partial x}\right)+\frac{\partial}{\partial y}\left(\mu_s\frac{\partial \theta}{\partial y}+\mu\frac{\partial T_s}{\partial y}\right)\right.\\&\left.+\frac{\partial}{\partial z}\left(\mu_s\frac{\partial \theta}{\partial z}\right)\right],\end{aligned} \tag{1e}$$

$$\begin{aligned}\Phi&=\mu_s\left[2\left(\frac{\partial u}{\partial y}+\frac{\partial v}{\partial x}\right)\left(\frac{\partial U_s}{\partial y}\right)+2\left(\frac{\partial v}{\partial z}+\frac{\partial w}{\partial y}\right)\left(\frac{\partial W_s}{\partial y}\right)\right]\\&+\mu\left[\left(\frac{\partial U_s}{\partial y}\right)^2+\left(\frac{\partial W_s}{\partial y}\right)^2\right],\end{aligned} \tag{1f}$$

$$\frac{\pi}{P_s}=\frac{\theta}{T_s}+\frac{\rho}{\rho_s}, \tag{1g}$$

where Re is the Reynolds number, Pr is the Prandtl number, and γ is the specific heat ratio. Additionally, $r=2(e+2)/3$, $m=2(e-1)/3$, where $e=0$ corresponds to the Stokes hypothesis. $U_s(y)$, $W_s(y)$, $T_s(y)$, and $\mu_s(y)$ are mean-flow profiles.

Denoting $\mathbf{A}=(u,\partial u/\partial y,v,\pi,\theta,\partial\theta/\partial y,w,\partial w/\partial y)^T$ as the disturbance vector function, it is possible to rewrite the system of equations (1a)–(1f) in the following matrix operator form:

$$\begin{aligned}\frac{\partial}{\partial y}\left(\mathbf{L}_0\frac{\partial \mathbf{A}}{\partial y}\right)+\frac{\partial \mathbf{A}}{\partial y}&=\mathbf{H}_{10}\frac{\partial \mathbf{A}}{\partial t}+\mathbf{H}_{11}\mathbf{A}+\mathbf{H}_2\frac{\partial \mathbf{A}}{\partial x}+\mathbf{H}_3\frac{\partial^2 \mathbf{A}}{\partial x\,\partial y}\\&+\mathbf{H}_4\frac{\partial^2 \mathbf{A}}{\partial x^2}+\mathbf{H}_5\frac{\partial \mathbf{A}}{\partial z}+\mathbf{H}_6\frac{\partial^2 \mathbf{A}}{\partial x\,\partial z}\\&+\mathbf{H}_7\frac{\partial^2 \mathbf{A}}{\partial y\,\partial z}+\mathbf{H}_8\frac{\partial^2 \mathbf{A}}{\partial z^2}.\end{aligned} \tag{2}$$

$\mathbf{L}_0$, $\mathbf{H}_{10}$, $\mathbf{H}_{11}$, $\mathbf{H}_2$, $\mathbf{H}_3$, $\mathbf{H}_4$, $\mathbf{H}_5$, $\mathbf{H}_6$, $\mathbf{H}_7$, and $\mathbf{H}_8$ are 8×8 matrices whose nonzero elements are presented in the Electronic Physics Auxiliary Publication Service (EPAPS).[12] At the initial time, $t=0$, the disturbance vector is denoted as

$$\mathbf{A}(x,y,z,0)=\mathbf{A}_0(x,y,z). \tag{3}$$

The boundary conditions are as follows:

$$\begin{aligned}&y=0:\quad u=v=w=\theta=0;\\&y\to\infty:\quad |A_j|\to 0\ (j=1,\ldots,8).\end{aligned} \tag{4}$$

These boundary conditions correspond to the no-slip condition and zero temperature disturbance on the wall, and all disturbances decaying to zero far outside the boundary layer.

III. SOLUTION OF THE INITIAL-VALUE PROBLEM

The three-dimensionality of both the boundary layer flow and the disturbance adds complexity to the problem. However, the problem can be solved using a similar approach to the one used in Ref. 3 for the 2D wave packet. The problem is solved using a Fourier transform with respect to

the streamwise coordinate, x, a Fourier transform with respect to the spanwise coordinate, z, and a Laplace transform with respect to time, t:

$$\mathbf{A}_{p\alpha\beta}(y) = \frac{1}{2\pi}\int_0^\infty e^{-pt}\int_{-\infty}^{\infty} e^{-i\alpha x}\int_{-\infty}^{\infty} e^{-i\beta z}\mathbf{A}(x,y,z,t)dzdxdt. \tag{5}$$

By applying the transforms given by Eq. (5) to the problem [Eqs. (2)–(4)], we arrive at a system of nonhomogeneous ordinary differential equations for the amplitude vector $\mathbf{A}_{p\alpha\beta}$:

$$\begin{aligned}\frac{d}{dy}\left(\mathbf{L}_0\frac{d\mathbf{A}_{p\alpha\beta}}{dy}\right) + \frac{d\mathbf{A}_{p\alpha\beta}}{dy} &= \mathbf{H}_{10}p\mathbf{A}_{p\alpha\beta} - \mathbf{H}_{10}\mathbf{A}_{0\alpha\beta} + \mathbf{H}_{11}\mathbf{A}_{p\alpha\beta} + i\alpha\mathbf{H}_2\mathbf{A}_{p\alpha\beta} \\ &+ i\alpha\mathbf{H}_3\frac{d\mathbf{A}_{p\alpha\beta}}{dy} - \alpha^2\mathbf{H}_4\mathbf{A}_{p\alpha\beta} + i\beta\mathbf{H}_5\mathbf{A}_{p\alpha\beta} - \alpha\beta\mathbf{H}_6\mathbf{A}_{p\alpha\beta} \\ &+ i\beta\mathbf{H}_7\frac{d\mathbf{A}_{p\alpha\beta}}{dy} - \beta^2\mathbf{H}_8\mathbf{A}_{p\alpha\beta},\end{aligned} \tag{6}$$

where $\mathbf{A}_{0\alpha\beta}(y)$ is the Fourier transform (with respect to both x and z) of $\mathbf{A}_0(x,y,z)$, the initial disturbance vector. The solution of Eq. (6) satisfies the following boundary conditions:

$$\begin{aligned}&y = 0: \quad A_{p\alpha\beta1} = A_{p\alpha\beta3} = A_{p\alpha\beta5} = A_{p\alpha\beta7} = 0; \\ &y \to \infty: \quad |A_{p\alpha\beta j}| \to 0 \ (j = 1,\ldots,8).\end{aligned} \tag{7}$$

The nonhomogeneous term in Eq. (6) is the term containing the Fourier transform of the initial disturbance, $\mathbf{A}_{0\alpha\beta}$. The remainder of the terms form the homogeneous part of Eq. (6). This homogeneous equation can be recast as the following system of ordinary differential equations:

$$\frac{d\mathbf{A}_{p\alpha\beta}}{dy} = \mathbf{H}_0\mathbf{A}_{p\alpha\beta}, \tag{8}$$

where $\mathbf{H}_0$ is an 8×8 matrix whose nonzero elements are presented in Ref. 12. There are eight fundamental solutions, $\mathbf{z}_1,\ldots,\mathbf{z}_8$, of the homogeneous system of equations given by Eq. (8). Outside the boundary layer ($y\to\infty$), $\mathbf{H}_0$ is a matrix of constant coefficients, and thus each fundamental solution has an exponential asymptotic behavior $\exp(\lambda_j y)$, where $\lambda_1,\ldots,\lambda_8$ are determined from the characteristic equation

$$\det\|\mathbf{H}_0 - \lambda\mathbf{I}\| = 0. \tag{9}$$

For $y\to\infty$, Eq. (9) can be written as

$$(b_{11}-\lambda^2)(b_{41}-\lambda^2)[(b_{22}-\lambda^2)(b_{33}-\lambda^2) - b_{23}b_{32}] = 0, \tag{10}$$

where

$$\begin{aligned}&b_{11} = H_0^{21}, \quad b_{41} = H_0^{87} = H_0^{21} = b_{11}, \\ &b_{22} = H_0^{42}H_0^{24} + H_0^{43}H_0^{34} + H_0^{46}H_0^{64} + H_0^{48}H_0^{84}, \\ &b_{23} = H_0^{42}H_0^{25} + H_0^{43}H_0^{35} + H_0^{46}H_0^{65} + H_0^{48}H_0^{85}, \\ &b_{32} = H_0^{64}, \quad b_{33} = H_0^{65},\end{aligned}$$

with $\mathbf{H}^{ij}$ denoting the (i,j) element of matrix $\mathbf{H}$.

The roots of Eq. (10) are

$$\begin{aligned}&\lambda_{1,2}^2 = b_{11} = \alpha^2 + \beta^2 + i\,\mathrm{Re}(\alpha + \beta W_{se} - ip), \\ &\lambda_{3,4}^2 = (b_{22}+b_{33})/2 + \tfrac{1}{2}\sqrt{(b_{22}-b_{33})^2 + 4b_{23}b_{32}}, \\ &\lambda_{5,6}^2 = (b_{22}+b_{33})/2 - \tfrac{1}{2}\sqrt{(b_{22}-b_{33})^2 + 4b_{23}b_{32}}, \\ &\lambda_{7,8}^2 = b_{41} = \alpha^2 + \beta^2 + i\,\mathrm{Re}(\alpha + \beta W_{se} - ip),\end{aligned} \tag{11}$$

where W_{se} is the mean-flow spanwise velocity at the upper boundary layer edge. The root branches are chosen to have $\mathrm{Real}(\lambda_1,\lambda_3,\lambda_5,\lambda_7) < 0$, and we define a matrix of fundamental solutions

$$\mathbf{Z} = \|\mathbf{z}_1,\ldots,\mathbf{z}_8\|. \tag{12}$$

The nonhomogeneous system given by Eq. (6) has a solution expressed in the form

$$\mathbf{A}_{p\alpha\beta} = \mathbf{Z}\mathbf{Q}(y), \tag{13}$$

where the vector of coefficients $\mathbf{Q}(y)$ is found using the method of variation of parameters:

$$\begin{aligned}2\mathbf{L}_0\frac{d\mathbf{Z}}{dy}\frac{d\mathbf{Q}}{dy} + \mathbf{L}_0\mathbf{Z}\frac{d^2\mathbf{Q}}{dy^2} + \frac{d\mathbf{L}_0}{dy}\mathbf{Z}\frac{d\mathbf{Q}}{dy} + \mathbf{Z}\frac{d\mathbf{Q}}{dy} - i\alpha\mathbf{H}_3\mathbf{Z}\frac{d\mathbf{Q}}{dy} \\ - i\beta\mathbf{H}_7\mathbf{Z}\frac{d\mathbf{Q}}{dy} = \mathbf{F},\end{aligned} \tag{14}$$

where $\mathbf{F} = -(\mathbf{H}_{10}\mathbf{A}_{0\alpha\beta})$. Since $\mathbf{Z}$ is the matrix of fundamental solutions of the homogeneous system of equations, it follows that $d\mathbf{Z}/dy = \mathbf{H}_0\mathbf{Z}$. Substitution of this relationship into Eq. (14) yields the following system of equations:

$$\begin{aligned}2\mathbf{L}_0\mathbf{H}_0\mathbf{Z}\frac{d\mathbf{Q}}{dy} + \mathbf{L}_0\mathbf{Z}\frac{d^2\mathbf{Q}}{dy^2} + \frac{d\mathbf{L}_0}{dy}\mathbf{Z}\frac{d\mathbf{Q}}{dy} + \mathbf{Z}\frac{d\mathbf{Q}}{dy} - i\alpha\mathbf{H}_3\mathbf{Z}\frac{d\mathbf{Q}}{dy} \\ - i\beta\mathbf{H}_7\mathbf{Z}\frac{d\mathbf{Q}}{dy} = \mathbf{F}.\end{aligned} \tag{15}$$

Let us consider the individual equations of Eq. (15). Denoting z_{ij} to be the ith component of vector $\mathbf{z}_j$, Q_j to be the jth component of vector $\mathbf{Q}$, and F_j to be the jth component of vector $\mathbf{F}$, then the first, third, fifth, sixth, and seventh equations of Eq. (15) are, respectively,

$$z_{1j}\frac{dQ_j}{dy}=0, \tag{16}$$

$$z_{3j}\frac{dQ_j}{dy}=F_3, \tag{17}$$

$$z_{5j}\frac{dQ_j}{dy}=0, \tag{18}$$

$$z_{6j}\frac{dQ_j}{dy}=F_6, \tag{19}$$

$$z_{7j}\frac{dQ_j}{dy}=0. \tag{20}$$

The second and eighth equations of Eq. (15) are, respectively,

$$z_{2j}\frac{dQ_j}{dy}-i\alpha H_3^{23}z_{3j}\frac{dQ_j}{dy}=F_2, \tag{21}$$

$$z_{8j}\frac{dQ_j}{dy}-i\beta H_7^{83}z_{3j}\frac{dQ_j}{dy}=F_8. \tag{22}$$

Substitution of Eq. (17) into Eq. (21) and Eq. (22) leads to the following forms:

$$z_{2j}\frac{dQ_j}{dy}=F_2+i\alpha H_3^{23}F_3, \tag{23}$$

$$z_{8j}\frac{dQ_j}{dy}=F_8+i\beta H_7^{83}F_3. \tag{24}$$

The fourth equation of Eq. (15) is

$$2L_0^{43}H_0^{3i}z_{ij}\frac{dQ_j}{dy}+L_0^{43}z_{3j}\frac{d^2Q_j}{dy^2}+z_{4j}\frac{dQ_j}{dy}+\frac{dL_0^{43}}{dy}z_{3j}\frac{dQ_j}{dy}=F_4. \tag{25}$$

By considering only the nonzero elements of H_0^{3i}, Eq. (25) can be rewritten as

$$z_{4j}\frac{dQ_j}{dy}=\frac{F_4-L_0^{43}H_0^{33}F_3-\dfrac{d(L_0^{43}F_3)}{dy}}{1+L_0^{43}H_0^{34}}. \tag{26}$$

Therefore, the nonhomogeneous system (15) can be rewritten as

$$\mathbf{Z}\frac{d\mathbf{Q}}{dy}=\boldsymbol{\varphi},$$

with

$$\varphi_1=0,\quad \varphi_2=-(\mathbf{H}_{10}\mathbf{A}_{0\alpha\beta})_2-i\alpha H_3^{23}(\mathbf{H}_{10}\mathbf{A}_{0\alpha\beta})_3,$$

$$\varphi_3=-(\mathbf{H}_{10}\mathbf{A}_{0\alpha\beta})_3,$$

$$\varphi_4=\frac{1}{1+L_0^{43}H_0^{34}}\left(-(\mathbf{H}_{10}\mathbf{A}_{0\alpha\beta})_4+L_0^{43}H_0^{33}(\mathbf{H}_{10}\mathbf{A}_{0\alpha\beta})_3+\frac{d[L_0^{43}(\mathbf{H}_{10}\mathbf{A}_{0\alpha\beta})_3]}{dy}\right), \tag{27}$$

$$\varphi_5=0,\quad \varphi_6=-(\mathbf{H}_{10}\mathbf{A}_{0\alpha\beta})_6,\quad \varphi_7=0,$$

$$\varphi_8=-(\mathbf{H}_{10}\mathbf{A}_{0\alpha\beta})_8-i\beta H_7^{83}(\mathbf{H}_{10}\mathbf{A}_{0\alpha\beta})_3.$$

The formal solution of Eq. (27) is expressed as

$$\mathbf{A}_{p\alpha\beta}=\sum_{j=1}^{8}\left(a_j+\int_{y_j}^{y}\frac{dQ_j}{dy}dy\right)\mathbf{z}_j, \tag{28}$$

where the constants a_j and y_j are determined using the boundary conditions given by Eq. (7). Using properties of determinants, we obtain the following solution:

$$\begin{aligned}\mathbf{A}_{p\alpha\beta}=&\left(a_1+\int_0^y\frac{dQ_1}{dy}dy\right)\mathbf{z}_1+\int_\infty^y\frac{dQ_2}{dy}dy\mathbf{z}_2\\&+\left(a_3+\int_0^y\frac{dQ_3}{dy}dy\right)\mathbf{z}_3+\int_\infty^y\frac{dQ_4}{dy}dy\mathbf{z}_4\\&+\left(a_5+\int_0^y\frac{dQ_5}{dy}dy\right)\mathbf{z}_5+\int_\infty^y\frac{dQ_6}{dy}dy\mathbf{z}_6\\&+\left(a_7+\int_0^y\frac{dQ_7}{dy}dy\right)\mathbf{z}_7+\int_\infty^y\frac{dQ_8}{dy}dy\mathbf{z}_8,\end{aligned} \tag{29a}$$

with

$$a_1=\frac{c_2E_{2357}+c_4E_{4357}+c_6E_{6357}+c_8E_{8357}}{E_{1357}}, \tag{29b}$$

$$a_3=\frac{c_2E_{1257}+c_4E_{1457}+c_6E_{1657}+c_8E_{1857}}{E_{1357}}, \tag{29c}$$

$$a_5=\frac{c_2E_{1327}+c_4E_{1347}+c_6E_{1367}+c_8E_{1387}}{E_{1357}}, \tag{29d}$$

$$a_7=\frac{c_2E_{1352}+c_4E_{1354}+c_6E_{1356}+c_8E_{1358}}{E_{1357}}, \tag{29e}$$

$$c_j=\int_0^\infty\frac{dQ_j}{dy}dy, \tag{29f}$$

$$E_{ijkl}=\det\begin{Vmatrix}z_{1i}&z_{1j}&z_{1k}&z_{1l}\\z_{3i}&z_{3j}&z_{3k}&z_{3l}\\z_{5i}&z_{5j}&z_{5k}&z_{5l}\\z_{7i}&z_{7j}&z_{7k}&z_{7l}\end{Vmatrix}_{y=0}. \tag{29g}$$

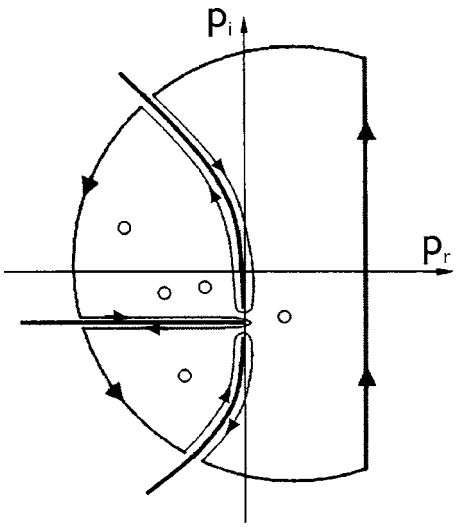

FIG. 1. Integration contour for the inverse Laplace transform.

IV. INVERSE LAPLACE TRANSFORM

The inverse Laplace transform of Eq. (29a) is

$$\mathbf{A}_{\alpha\beta}(y,t;\alpha,\beta) = \frac{1}{2\pi i}\int_{p_0-i\infty}^{p_0+i\infty} \mathbf{A}_{p\alpha\beta}(y;p,\alpha,\beta)e^{pt}dp. \qquad (30)$$

Figure 1 shows a schematic of an appropriate integration contour for the inverse Laplace transform, which is determined by poles (relevant to the discrete spectrum) and by branch cuts (relevant to the continuous spectrum).

By integrating along the contour shown in Fig. 1, Eq. (30) can be written as a sum of integrals along the sides, γ^+ and γ^-, of each branch cut and a sum of residues resulting from the poles of Eq. (29a) given by the equation $E_{1357}(p)=0$, i.e.,

$$\mathbf{A}_{\alpha\beta} = -\frac{1}{2\pi i}\sum_m \left(\int_{\gamma_m^+} \mathbf{A}_{p\alpha\beta}e^{pt}dp + \int_{\gamma_m^-} \mathbf{A}_{p\alpha\beta}e^{pt}dp\right) + \sum_n \mathrm{Res}_n(\mathbf{A}_{p\alpha\beta}e^{pt}). \qquad (31)$$

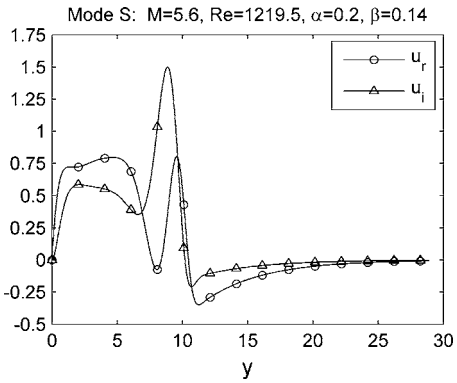

FIG. 2. Streamwise velocity disturbance of mode S.

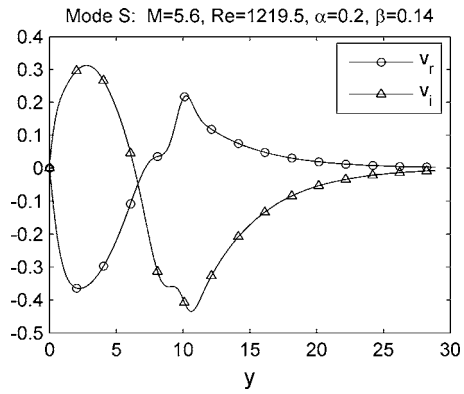

FIG. 3. Normal velocity disturbance of mode S.

A. Discrete spectrum

Modes of the discrete spectrum correspond to poles of Eq. (29a), which are roots of $E_{1357}(p)=0$, where E_{1357} is defined by Eq. (29g). Discrete modes arise from the situation when all the roots of Eq. (11) have nonzero real parts and are given by the poles' contribution to the inverse Laplace transform, i.e., the residues shown in Eq. (31). These residues have the form

$$\mathrm{Res}_n(\mathbf{A}_{p\alpha\beta}e^{pt}) = \mathbf{A}_n(y;p_n,\alpha,\beta)e^{p_n t}, \qquad (32)$$

with

$$\mathbf{A}_n = [\hat{a}_1\mathbf{z}_1 + \hat{a}_3\mathbf{z}_3 + \hat{a}_5\mathbf{z}_5 + \hat{a}_7\mathbf{z}_7]\left(\frac{\partial E_{1357}}{\partial p}(p_n)\right)^{-1}, \qquad (33)$$

where $\hat{a}_1$, $\hat{a}_3$, $\hat{a}_5$, and $\hat{a}_7$ are given by the numerators of Eqs. (29b)–(29e). If the eigenvalue $p_n=-i\omega_n$ belongs to the discrete spectrum, then the associated eigenfunction $\mathbf{A}_n$ decays exponentially outside the boundary layer ($y\to\infty$).

To illustrate features of the spectrum, we consider a boundary layer over an adiabatic sharp cone at zero angle of attack. The length scale is $L^*=\sqrt{(\mu_e^* x^*/\rho_e^* U_e^*)}$ and the Reynolds number is $\mathrm{Re}=\sqrt{(\rho_e^* U_e^* x^*/\mu_e^*)}$. Using the Lees-Dorodnitsyn transformation,[13] we solve the conical problem with boundary layer profiles for a flat plate. Accordingly, all conical results presented hereafter can be adjusted to the flat plate boundary layer by dividing the parameters Re, α, β, and ω by $\sqrt{3}$.

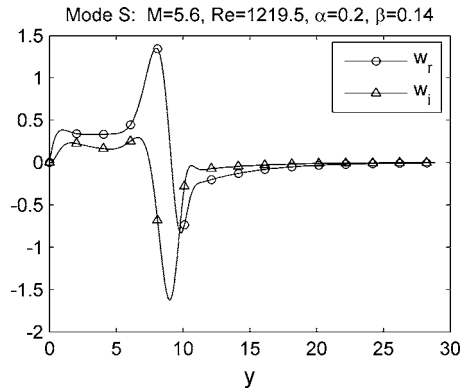

FIG. 4. Spanwise velocity disturbance of mode S.

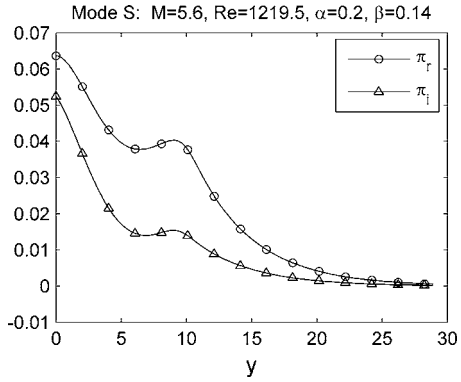

FIG. 5. Pressure disturbance of mode S.

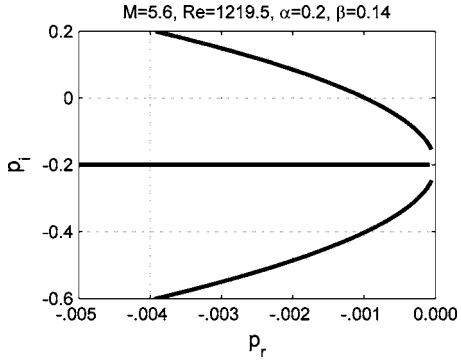

FIG. 7. Branch cuts of the continuous spectrum in the complex plane $p=-i\omega$.

The standard form for the direct problem given by Eq. (8) was used for the numerical evaluations. The numerical scheme performs the integration of Eq. (8) for four fundamental solutions (discrete spectrum) or for five fundamental solutions (continuous spectrum). A fourth-order Runge–Kutta integration method with constant step (301 points) was used to integrate from outside the boundary layer ($y_{\max}=25$) toward the wall using the Gram-Schmidt orthonormalization procedure.

When analyzing the continuous spectrum, k is a parameter, and the frequency ω is calculated using $\lambda_j^2=-k^2$, where λ_j are given by Eq. (11). When analyzing the discrete spectrum, ω is calculated using Newton's iteration method. This iteration method depends on the initial approach to ω. A two-domain Chebyshev spectral collocation method[14] was used to determine the initial approach.

To maintain consistency with the 2D problem analyzed in Ref. 3, we choose the following parameter values: $M=5.6$, Re=1219.5, Pr=0.7, $\gamma=1.4$, $e=0$ with an adiabatic wall and stagnation temperature $T_0=470$ K.

Two discrete modes are of interest. One discrete mode will be referred to as "mode F," where "F" stands for "fast"; this is the mode whose phase speed approaches that of the fast acoustic mode as $\alpha\to 0$ (2D case). Another discrete mode will be referred to as "mode S," where "S" stands for "slow"; this is the mode whose phase speed approaches that of the slow acoustic mode as $\alpha\to 0$ (2D case). Even though in the 3D case, synchronism with the fast and slow acoustic modes as $\alpha\to 0$ may no longer occur, the behavior of each mode curve (3D) is similar to the behavior of the corresponding 2D mode curve. Thus it should not be confusing to refer to the 3D curves as mode F and mode S.

As an example, Figs. 2, 3, and 4 show the distribution for the streamwise, normal, and spanwise velocity disturbances corresponding to mode S for $\alpha=0.2$, $\beta=0.14$, with complex-valued eigenvalue $\omega=0.18291+i3.95\times 10^{-5}$ (this choice of parameters corresponds to a disturbance propagation angle of $\psi\approx 35°$, where $\tan\psi=\beta/\alpha$). Figures 5 and 6 show respectively the pressure and temperature disturbances corresponding to this mode.

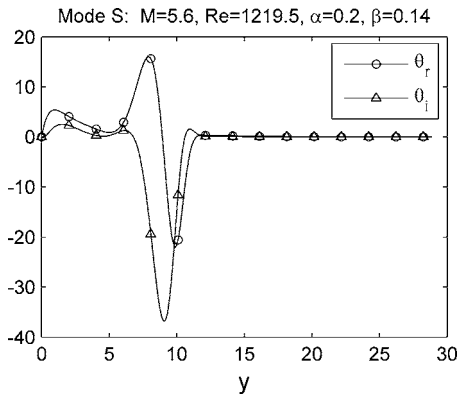

FIG. 6. Temperature disturbance of mode S.

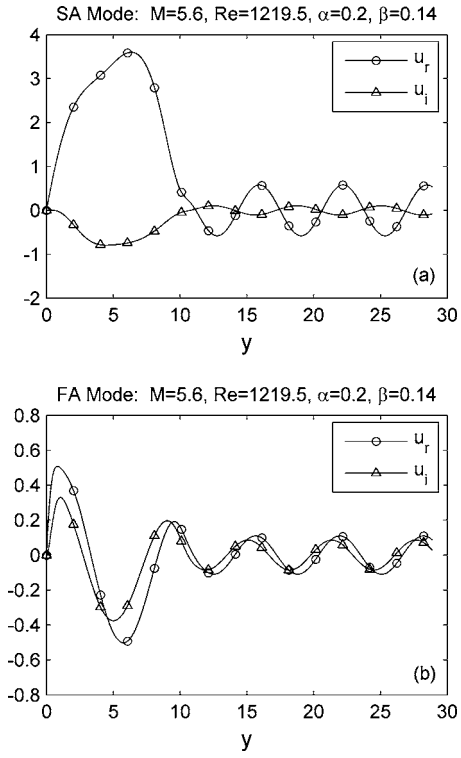

FIG. 8. Streamwise velocity disturbance of the acoustic mode: (a) slow, (b) fast.

B. Continuous spectrum

Modes of the continuous spectrum correspond to branch cuts of Eq. (29a). Solutions of the continuous spectrum arise from the situation when a characteristic number λ_j given by Eq. (11) is purely imaginary ($\lambda_j^2=-k^2$, $k>0$, $j=1, \ldots, 8$). As in the 2D case discussed in Ref. 3, the first pure oscillatory solution corresponds to $\lambda_{1,2}^2=-k^2$. This equation, along with Eq. (11), leads to the following (different from the 2D case) relation:

$$p_{c,1}=-i(\alpha+\beta W_{se})-(k^2+\alpha^2+\beta^2)/\mathrm{Re}. \tag{34}$$

As in the 2D case, this solution is interpreted as a vorticity branch, where the vorticity disturbances are propagating with a phase speed of $c=1$. The equation

$$[(b_{22}-\lambda^2)(b_{33}-\lambda^2)-b_{23}b_{32}]=0 \tag{35}$$

is a third-degree polynomial in p and has three roots at $\lambda^2=-k^2$. These roots $(p_{c,2},p_{c,3},p_{c,4})$ were computed numerically for the case when $W_{se}=0$ (2D mean flow). Figure 7 shows the results for $\alpha=0.2$, $\beta=0.14$. The horizontal branch in Fig. 7 has a finite limiting point and is interpreted as an entropy branch, where the entropy disturbances are propagating with a phase speed of $c=1$. The vorticity branch given by Eq. (34) overlaps the entropy branch. The upper and lower branches in Fig. 7 are associated with fast and slow acoustic waves. These waves travel with the respective phase speeds $c=1\pm\sqrt{1+\beta^2/\alpha^2}/M_e$. The fifth pure oscillatory solution is an additional solution not found for the 2D case. The equation, $\lambda_{7,8}^2=-k^2$, along with Eq. (11), leads to the relation

$$p_{c,5}=-i(\alpha+\beta W_s)-(k^2+\alpha^2+\beta^2)/\mathrm{Re}. \tag{36}$$

Equation (36) is identical to Eq. (34). The fifth relation is also interpreted as a vorticity branch, where the vorticity disturbances are propagating with a phase speed of $c=1$. The existence of two vorticity modes reflects the three-dimensionality of the perturbations.

As in the 2D case, it is possible to find compact forms for the solutions of the various regions of the continuous spectrum. Using a similar technique to that used in Ref. 3, we denote one side of each branch cut as plus (+) and the other side of the branch cut as minus (−) in accordance with the asymptotic behavior of the type of disturbance being considered. By relating $\mathbf{z}_j^+$ to $\mathbf{z}_j^-$ and dQ_j^+/dy to dQ_j^-/dy, the integrals along the branch cut sides γ^+ and γ^- can be written as one integral of the difference $\mathbf{A}_{p\alpha\beta}^+-\mathbf{A}_{p\alpha\beta}^-$.

Solutions for the acoustic waves include five fundamental vector functions, three of which decay outside the boundary layer, and two of which oscillate as $e^{\pm iky}$. $\mathbf{A}_{p\alpha\beta}^+-\mathbf{A}_{p\alpha\beta}^-$ can be written solely in terms of the functions on the + side of the branch cut as

$$\begin{aligned}\mathbf{A}_{p\alpha\beta}^+-\mathbf{A}_{p\alpha\beta}^-=&\left(\frac{c_2E_{1275}}{E_{1753}E_{1754}}+\frac{c_3E_{1753}}{E_{1753}E_{1754}}+\frac{c_4E_{1754}}{E_{1753}E_{1754}}\right.\\&\left.+\frac{c_6E_{1756}}{E_{1753}E_{1754}}+\frac{c_8E_{7185}}{E_{1753}E_{1754}}\right)(E_{5734}\mathbf{z}_1\\&+E_{1754}\mathbf{z}_3+E_{7153}\mathbf{z}_4+E_{7134}\mathbf{z}_5+E_{1534}\mathbf{z}_7).\end{aligned} \tag{37}$$

The horizontal branch cut in the 2D case has a region of overlapping vorticity and entropy disturbances. The remainder of the branch cut is a region of vorticity disturbances. In the 3D problem, the entire branch cut contains a region of overlapping vorticity modes, and there is a region of the branch cut that has entropy disturbances overlapping the two vorticity modes.

In the region of overlapping vorticity modes, there is an uncertainty. There are six fundamental solutions (four oscillating and two decaying) in this region; however, this number of fundamental solutions is larger than is needed to satisfy the boundary conditions. This difficulty is resolved using the technique described above in obtaining Eq. (37). The solution can be expressed as a sum of two standalone vorticity modes as follows:

$$\mathbf{A}_{p\alpha\beta}^+-\mathbf{A}_{p\alpha\beta}^-=\mathbf{A}_{c,1}+\mathbf{A}_{c,5}, \tag{38}$$

where

$$\begin{aligned}\mathbf{A}_{c,1}=&\left(\frac{c_1E_{1753}}{E_{1753}E_{2753}}+\frac{c_2E_{2753}}{E_{1753}E_{2753}}+\frac{c_4E_{4753}}{E_{1753}E_{2753}}\right.\\&\left.+\frac{c_6E_{6753}}{E_{1753}E_{2753}}+\frac{c_8E_{8753}}{E_{1753}E_{2753}}\right)(E_{2753}\mathbf{z}_1-E_{1753}\mathbf{z}_2\\&+E_{1275}\mathbf{z}_3+E_{1723}\mathbf{z}_5+E_{1253}\mathbf{z}_7)\end{aligned} \tag{39}$$

and

$$\begin{aligned}\mathbf{A}_{c,5}=&\left(\frac{c_1E_{1253}}{E_{2753}E_{2853}}+\frac{c_4E_{5234}}{E_{2753}E_{2853}}+\frac{c_6E_{2563}}{E_{2753}E_{2853}}\right.\\&\left.+\frac{c_7E_{7253}}{E_{2753}E_{2853}}+\frac{c_8E_{8253}}{E_{2753}E_{2853}}\right)(E_{7853}\mathbf{z}_2+E_{2785}\mathbf{z}_3\\&-E_{2783}\mathbf{z}_5-E_{2853}\mathbf{z}_7+E_{2753}\mathbf{z}_8).\end{aligned} \tag{40}$$

Both Eqs. (39) and (40) satisfy the boundary conditions on the wall.

In the region of three overlapping modes (two vorticity and entropy), there also exists an uncertainty. There are seven fundamental solutions in this region (six oscillating and one decaying). Again, this number of fundamental solutions is larger than is needed to satisfy the boundary conditions. This difficulty is resolved using the technique described previously in obtaining Eq. (37), and since the region of three overlapping modes has not been encountered before, we shall show the derivation of the solution. In this overlapping region, we denote one side of the branch cut as + and the other side of the branch cut as − in accordance with the asymptotic behavior:

$$\mathbf{z}_1^+\sim e^{iky},\quad \mathbf{z}_1^-\sim e^{-iky},\quad \mathbf{z}_2^+\sim e^{-iky}, \tag{41a}$$

$$\mathbf{z}_2^-\sim e^{iky},\quad \mathbf{z}_3^+\sim e^{\lambda_3 y},\quad \mathbf{z}_3^-\sim e^{\lambda_3 y}, \tag{41b}$$

$$\mathbf{z}_4^+\sim e^{\lambda_4 y},\quad \mathbf{z}_4^-\sim e^{\lambda_4 y},\quad \mathbf{z}_5^+\sim e^{ik_1 y}, \tag{41c}$$

$$\mathbf{z}_5^-\sim e^{-ik_1 y},\quad \mathbf{z}_6^+\sim e^{-ik_1 y},\quad \mathbf{z}_6^-\sim e^{ik_1 y}, \tag{41d}$$

$$\mathbf{z}_7^+ \sim e^{iky}, \quad \mathbf{z}_7^- \sim e^{-iky}, \quad \mathbf{z}_8^+ \sim e^{-iky}, \quad \mathbf{z}_8^- \sim e^{iky}, \tag{41e}$$

where k and k_1 are real, positive parameters, and $\lambda_{3,4}$ are given by Eq. (11). It is possible to obtain the relations

$$\mathbf{z}_1^- = \mathbf{z}_2^+, \quad \mathbf{z}_2^- = \mathbf{z}_1^+, \quad \mathbf{z}_3^- = \mathbf{z}_3^+, \quad \mathbf{z}_4^- = \mathbf{z}_4^+, \tag{42a}$$

$$\mathbf{z}_5^- = \mathbf{z}_6^+, \quad \mathbf{z}_6^- = \mathbf{z}_5^+, \quad \mathbf{z}_7^- = \mathbf{z}_8^+, \quad \mathbf{z}_8^- = \mathbf{z}_7^+, \tag{42b}$$

$$\frac{dQ_1^-}{dy} = \frac{dQ_2^+}{dy}, \quad \frac{dQ_2^-}{dy} = \frac{dQ_1^+}{dy}, \tag{42c}$$

$$\frac{dQ_3^-}{dy} = \frac{dQ_3^+}{dy}, \quad \frac{dQ_4^-}{dy} = \frac{dQ_4^+}{dy}, \tag{42d}$$

$$\frac{dQ_5^-}{dy} = \frac{dQ_6^+}{dy}, \quad \frac{dQ_6^-}{dy} = \frac{dQ_5^+}{dy}, \tag{42e}$$

$$\frac{dQ_7^-}{dy} = \frac{dQ_8^+}{dy}, \quad \frac{dQ_8^-}{dy} = \frac{dQ_7^+}{dy}. \tag{42f}$$

The integrals along the branch cut sides γ^+ and γ^- can be written as one integral of the difference

$$\begin{aligned}
\mathbf{A}_{p\alpha\beta}^+ - \mathbf{A}_{p\alpha\beta}^- = &\left(a_1^+ + \int_0^y \frac{dQ_1^+}{dy}dy\right)\mathbf{z}_1^+ + \int_\infty^y \frac{dQ_2^+}{dy}dy\mathbf{z}_2^+ \\
&+ \left(a_3^+ + \int_0^y \frac{dQ_3^+}{dy}dy\right)\mathbf{z}_3^+ + \int_\infty^y \frac{dQ_4^+}{dy}dy\mathbf{z}_4^+ \\
&+ \left(a_5^+ + \int_0^y \frac{dQ_5^+}{dy}dy\right)\mathbf{z}_5^+ + \int_\infty^y \frac{dQ_6^+}{dy}dy\mathbf{z}_6^+ \\
&+ \left(a_7^+ + \int_0^y \frac{dQ_7^+}{dy}dy\right)\mathbf{z}_7^+ + \int_\infty^y \frac{dQ_8^+}{dy}dy\mathbf{z}_8^+ \\
&- \left(a_1^- + \int_0^y \frac{dQ_1^-}{dy}dy\right)\mathbf{z}_1^- - \int_\infty^y \frac{dQ_2^-}{dy}dy\mathbf{z}_2^- \\
&- \left(a_3^- + \int_0^y \frac{dQ_3^-}{dy}dy\right)\mathbf{z}_3^- - \int_\infty^y \frac{dQ_4^-}{dy}dy\mathbf{z}_4^- \\
&- \left(a_5^- + \int_0^y \frac{dQ_5^-}{dy}dy\right)\mathbf{z}_5^- - \int_\infty^y \frac{dQ_6^-}{dy}dy\mathbf{z}_6^- \\
&- \left(a_7^- + \int_0^y \frac{dQ_7^-}{dy}dy\right)\mathbf{z}_7^- - \int_\infty^y \frac{dQ_8^-}{dy}dy\mathbf{z}_8^-.
\end{aligned} \tag{43}$$

After substitution of the relations given in Eqs. (41a)–(41e) and (42a)–(42f), simplification leads to the following expression:

$$\begin{aligned}
\mathbf{A}_{p\alpha\beta}^+ - \mathbf{A}_{p\alpha\beta}^- = &(a_1^+ + c_1^+)\mathbf{z}_1^+ - (c_2^+ + a_1^-)\mathbf{z}_2^+ + (a_3^+ - a_3^-)\mathbf{z}_3^+ \\
&+ (a_5^+ + c_5^+)\mathbf{z}_5^+ - (a_5^- + c_6^+)\mathbf{z}_6^+ + (a_7^+ + c_7^+)\mathbf{z}_7^+ \\
&- (c_8^+ + a_7^-)\mathbf{z}_8^+.
\end{aligned} \tag{44}$$

Equation (44) can be expressed in the compact form

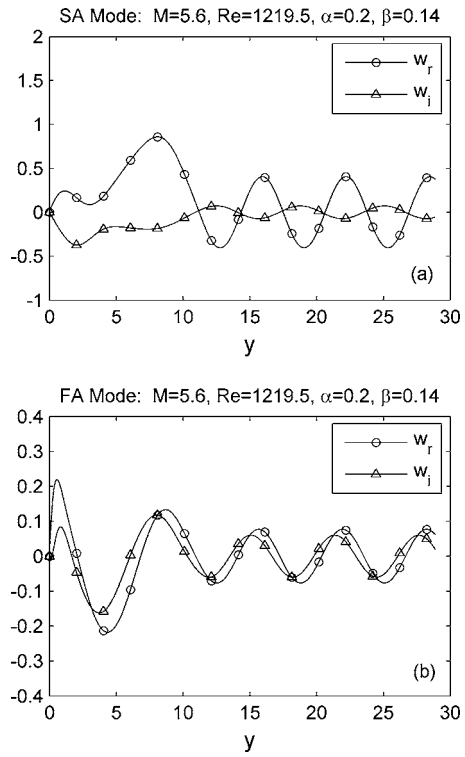

FIG. 9. Spanwise velocity disturbance of the acoustic mode: (a) slow, (b) fast.

$$\mathbf{A}_{p\alpha\beta}^+ - \mathbf{A}_{p\alpha\beta}^- = \mathbf{A}_{c,1} + \mathbf{A}_{c,2} + \mathbf{A}_{c,5}, \tag{45}$$

where $\mathbf{A}_{c,1}$ and $\mathbf{A}_{c,5}$ are given by Eqs. (39) and (40) and with

$$\begin{aligned}
\mathbf{A}_{c,2} = &\left(\frac{c_1 E_{1283}}{E_{2853}E_{2863}} - \frac{c_4 E_{2834}}{E_{2853}E_{2863}} + \frac{c_5 E_{2853}}{E_{2853}E_{2863}}\right. \\
&\left. + \frac{c_6 E_{2863}}{E_{2853}E_{2863}} - \frac{c_7 E_{2783}}{E_{2853}E_{2863}}\right)(E_{8563}\mathbf{z}_2 + E_{2856}\mathbf{z}_3 \\
&+ E_{2863}\mathbf{z}_5 - E_{2853}\mathbf{z}_6 - E_{2563}\mathbf{z}_8).
\end{aligned} \tag{46}$$

Each term in Eq. (45) satisfies the boundary conditions on the wall and can be interpreted as a standalone mode.

As an example, Figs. 8 and 9 show the distribution of the streamwise and spanwise velocity for both slow and fast acoustic disturbances.

C. Summary

We can now express the inverse Laplace transform given by Eq. (31) as

$$\begin{aligned}
\mathbf{A}_{\alpha\beta}(y,t;\alpha,\beta) = &-\frac{1}{2\pi i}\sum_{m=1}^{5}\int_0^\infty \mathbf{A}_{c,m}(y;k,\alpha,\beta) \\
&\times e^{p_{c,m}(k)t}\frac{dp_{c,m}}{dk}dk + \sum_n \mathbf{A}_n(y;p_n,\alpha,\beta)e^{p_n t},
\end{aligned} \tag{47}$$

where $m=1$ corresponds to one vorticity wave, with $p_{c,1}$ and $\mathbf{A}_{c,1}$ given by Eqs. (34) and (39), respectively; $m=2$ corresponds to the entropy wave, with $p_{c,2}$ and $\mathbf{A}_{c,2}$ given by Eqs. (35) and (46), respectively; $m=3,4$ correspond to slow and

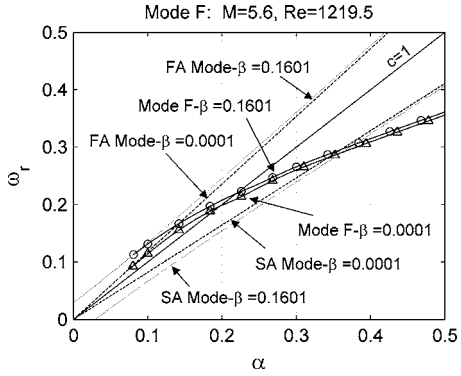

FIG. 10. Eigenvalues for mode F for $\beta=0.0001$ and $\beta=0.1601$.

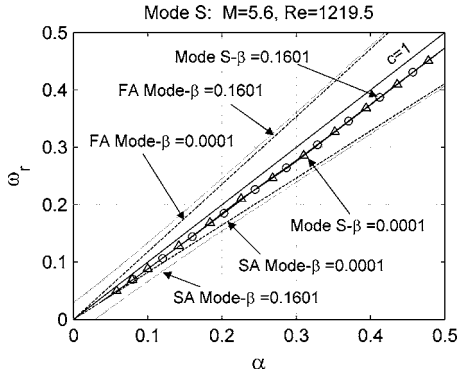

FIG. 12. Eigenvalues for mode S for $\beta=0.0001$ and $\beta=0.1601$.

fast acoustic waves, with $p_{c,3,4}$ and $\mathbf{A}_{c,3,4}$ given by Eqs. (35) and (37), respectively; $m=5$ corresponds to the second vorticity wave, with $p_{c,5}$ and $\mathbf{A}_{c,5}$ given by Eqs. (36) and (40), respectively; p_n is a root of $E_{1357}(p)=0$, and $\mathbf{A}_n$ is given by Eq. (33).

D. Biorthogonal system of eigenfunctions

Following Ref. 15, it is possible to express a solution of the initial-value problem [Eq. (47)] as an expansion in the biorthogonal eigenfunction system $\{\mathbf{A}_\omega, \mathbf{B}_\omega\}$, where the vector $\mathbf{A}_\omega$ is a solution of the direct problem and the vector $\mathbf{B}_\omega$ is a solution of the adjoint problem. There is an orthogonality relation associated with the biorthogonal eigenfunction system. This orthogonality relation, along with the Fourier transform of the initial data, can be used to compute the coefficients associated with each of the discrete and continuous modes. Further details can be found in the Appendix.

V. SYNCHRONISM OF MODE S AND MODE F WITH ACOUSTIC WAVES

In the 2D problem, mode S and mode F are synchronized respectively with the slow and fast acoustic modes for a wave number $\alpha \to 0$. Figure 10 shows numerical results for eigenvalues ω_r of mode F for a fixed choice of spanwise wave number β. Included in Fig. 10 are lines of constant phase speed. One of these is a line of phase speed $c=1$, the speed at which the entropy and vorticity disturbances travel. The other lines are associated with fast acoustic modes (FA mode) and slow acoustic modes (SA mode) for $\beta=0.0001$ (2D) and $\beta=0.1601$. The fast/slow acoustic waves travel with phase speed $c=1\pm\sqrt{1+\beta^2/\alpha^2}/M_e$. Figure 10 shows that mode F for both $\beta=0.0001$ and $\beta=0.1601$ is a subsonic disturbance relative to the free stream for $\alpha<0.37$ and is a supersonic disturbance relative to the free stream for $\alpha>0.37$. Furthermore, although it is not shown in any figure, these disturbances are everywhere decaying. To obtain a clearer picture of what is occurring at the lower wave numbers, Fig. 11 shows a section of Fig. 10.

As can be seen in Fig. 11, just as mode F at $\beta=0.0001$ is synchronized with the $\beta=0.0001$ fast acoustic mode at a wave number $\alpha<0.1$, mode F at $\beta=0.1601$ is synchronized with the $\beta=0.1601$ fast acoustic modes at a wave number $\alpha<0.1$.

Figure 12 shows numerical results for eigenvalues ω_r of mode S for a fixed choice of spanwise wave number. Also included in Fig. 12 are lines of constant phase speed for the FA mode and SA mode for $\beta=0.0001$ and $\beta=0.1601$. The two mode S curves are virtually overlapping. In order to gain a clearer view of what is occurring at the lower wave numbers, Fig. 13 shows a section of Fig. 12.

In contrast to mode F, Fig. 13 clearly shows that mode S for both choices of β is asymptotically approaching the SA mode for $\beta=0.0001$. We have observed this behavior at every choice of β that we have checked. Even though mode S for various choices of β (3D) approach the SA mode for $\beta=0.0001$, there is no synchronism between the two. The pri-

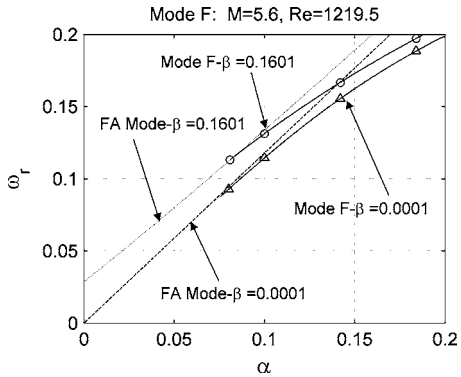

FIG. 11. Figure 10 at low wave number.

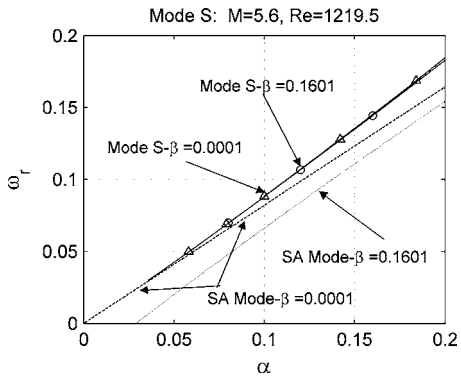

FIG. 13. Figure 12 at low wave number.

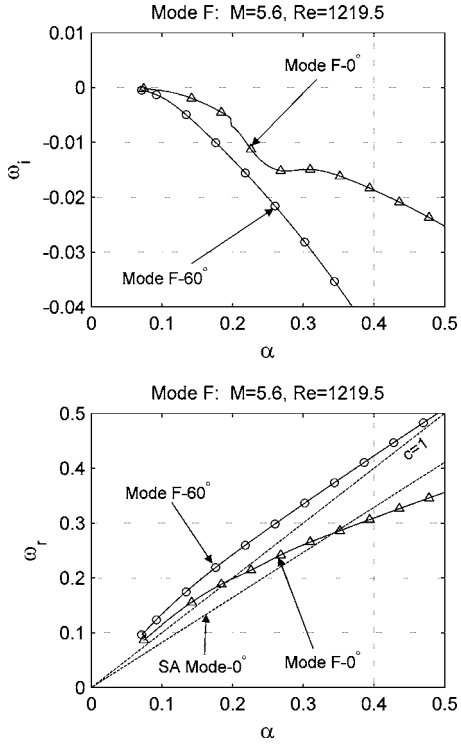

FIG. 14. Eigenvalues for mode F for $\psi=0^{\circ}$ and $\psi=60^{\circ}$.

mary synchronism of mode S with acoustic waves for $\alpha < 0.1$ is two-dimensional (2D mode S with the 2D SA mode).

VI. SYNCHRONISM OF MODE F WITH ENTROPY AND VORTICITY WAVES

Figure 14 shows eigenvalues of mode F for $\psi=0°$ and $\psi=60°$. One can see that for $\psi=0°$, mode F is subsonic relative to the free stream for $\alpha<0.35$ and is supersonic relative to the free stream for $\alpha>0.35$. However, for $\psi=60°$, mode F is subsonic relative to the free stream for this entire range of α. It can also be seen that mode F for both angles of disturbance propagation is everywhere decaying.

Furthermore, Fig. 14 shows the synchronism between the 2D mode F and the entropy and vorticity modes of the phase speed $c=1$. In the 2D case, as the discrete mode coalesces with the continuous spectrum from one side of the branch cut, it reappears on the other side at another point. Mathematically, the pole associated with mode F approaches one side of the branch cut on the complex p plane. At the same time, another pole, located on the lower Riemann sheet, approaches the branch cut from the opposite side. As the pole on the plane coalesces with the branch cut, it moves to the upper Riemann sheet, while simultaneously, the pole that was on the lower Riemann sheet moves into the complex p plane at another point.[3] This leads to a jump in ω_i. As the angle increases, the synchronism continues, but the jump size decreases, until it is seen that for $\psi=60°$ there is neither a synchronism, nor a jump in ω_i, at least for this interval of wave number α. Figure 15 shows contours of ω_i in the $\alpha-\beta$ wave number plane. One can see the jump location for choices of α and β. Also plotted in the figure is a small

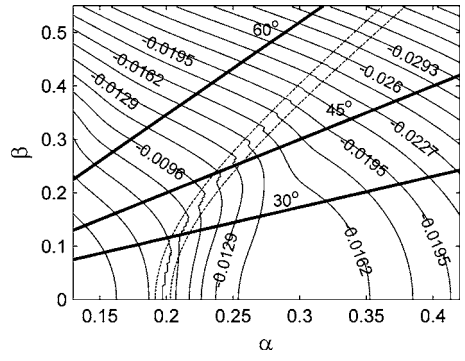

FIG. 15. Contours of ω_i in the $\alpha-\beta$ plane.

region bounding the branch cut. This region is denoted by the dashed lines. We have done this in lieu of plotting the branch cut, since the branch cut plot obscures the jumps in ω_i. It is clear that the discontinuity of ω_i is associated with the synchronism of mode F and the entropy and vorticity waves. For large values of β, it appears that no jump is seen in Fig. 15 at the location of the branch cut. A jump does in fact exist, but the size of the jump is small enough so that it cannot be seen on the scale of this figure.

By plotting lines of constant angle, it is seen that the synchronism between mode F and the entropy and vorticity waves vanishes for large enough angles.

VII. SYNCHRONISM OF MODE S WITH MODE F

Figure 16 shows the eigenvalue curves for mode S and mode F for $\psi=30°$. The mode S curve given by the imaginary part of the eigenvalue ω_i contains two regions of insta-

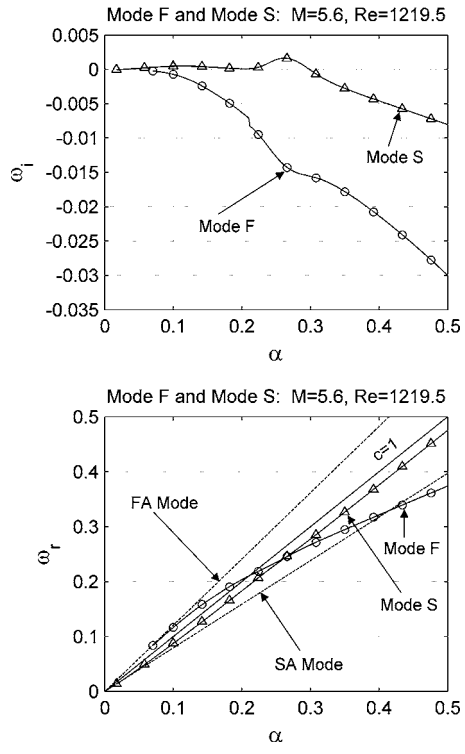

FIG. 16. Eigenvalues for mode F and mode S for $\psi=30^{\circ}$.

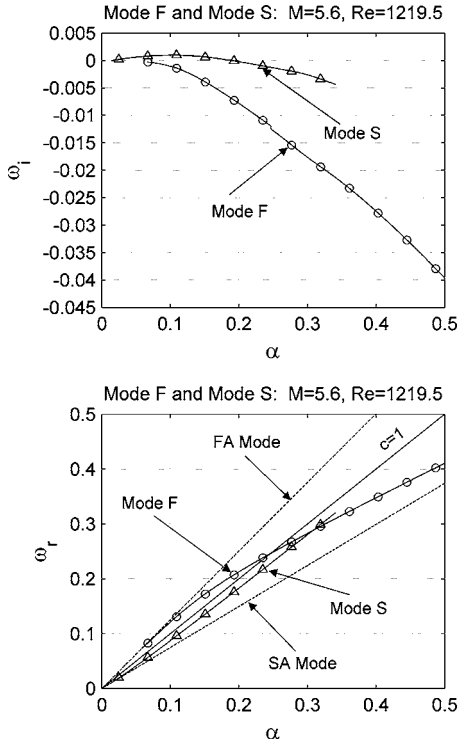

FIG. 17. Eigenvalues for mode F and mode S for $\psi=45^\circ$.

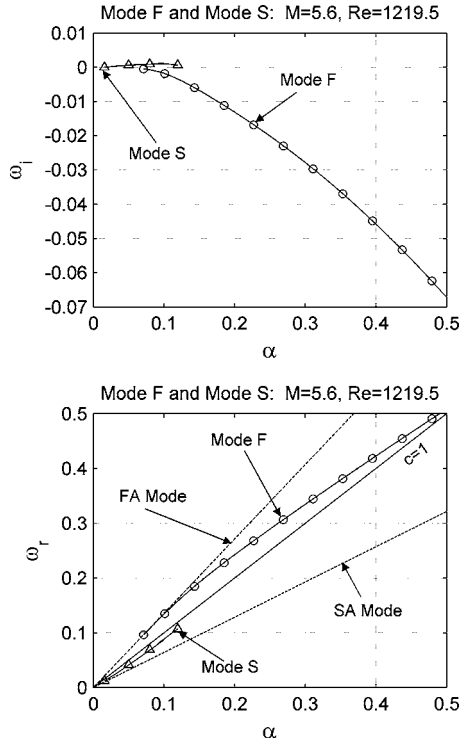

FIG. 18. Eigenvalues for mode F and mode S for $\psi=60^\circ$.

bility. The unstable region located at $\alpha=0.12$ is equivalent to Mack's first mode. The unstable region located at $\alpha=0.26$ is equivalent to Mack's second mode. Further details regarding the relation between mode S and mode F and Mack's acoustic modes can be found in Sec. VIII. The range of α is extended to $\alpha=0.5$ in order to show the decaying behavior of both mode S and mode F for larger values of α.

In the 2D case, mode F is synchronized with mode S. This synchronism is indicative of the fact that the discrete spectrum has a branch point at α^* in the complex α plane. True synchronism (mode S and mode F have the same value of ω_i as well as the same value of ω_r) occurs at α^*, which may have a different real part from where mode S's value of ω_r is equal to mode F's value of ω_r. At values of $\alpha > \alpha_r^*$, the disturbance spectrum branches out: mode S becomes unstable while mode F becomes more stable (the topological pattern may be sensitive to the mean flow parameters, such as Mach number, Prandtl number, and temperature factor; further details can be found in Ref. 11).

As seen in Fig. 16, this mode S instability continues for a disturbance propagating at $\psi=30^\circ$ (near $\alpha\approx0.23$). For larger angles, however, even though there is still synchronism between mode S and mode F, the synchronism is no longer accompanied by a mode S instability. This behavior can be seen for a disturbance propagating at $\psi=45^\circ$ in Fig. 17. Even though it cannot be seen in Fig. 17, plots of the pressure disturbance indicate that there is a switch from the Mack first mode to the Mack second mode. However, for this disturbance propagation angle, there is no amplified Mack second mode.

In Fig. 18, one can see that at even higher angles of disturbance propagation, there is no synchronism between mode S and mode F. Additionally, at this angle, the mode S curve consists entirely of the Mack first mode.

VIII. DISCUSSION

In order to avoid confusion, we now discuss Mack's[8,9] results and how they relate to mode S and mode F. Mack first considered inviscid perturbations and computed eigenvalue curves or families for various choices of parameters. Each of these families contains an unstable region corresponding to one of the higher Mack modes (first mode, second mode, third mode, etc.), and each amplification rate curve represents a distinct discrete mode. Using asymptotic analysis, Gushchin and Fedorov[16] also captured the feature that each amplified first mode, second mode, etc. represents a separate solution.

Mack then considered viscous perturbations and computed families of eigenvalues for finite Reynolds numbers and compared the eigenvalue curves with the inviscid ones. For one of Mack's choices of parameters, there were two "separate … inviscid amplification rate curves for the first and second modes" (Ref. 8, pp. 12–24) (i.e., two inviscid normal modes), but "only a single amplification rate curve at the finite Reynolds number shown" (Ref. 8, pp. 12–24) (i.e., one viscous normal mode). This one viscous solution was comprised of both the first mode and the second mode. This viscous family is analogous to the mode S mentioned in prior sections. Mode S in our analysis is a single discrete mode that corresponds to a single pole in the complex p plane. Furthermore, mode S is comprised of Mack's amplified first, second, and possibly higher modes.

Additionally, Mack explained how "the inviscid solutions are to be the $\mathrm{Re}\to\infty$ limit of the viscous solutions" (Ref. 8, pp. 12–25) through "the existence of multiple viscous solutions" (Ref. 8, pp. 12–25). For the Reynolds number of his example, this additional viscous solution is damped, and it is analogous to the mode F mentioned in prior sections. We would like to point out that Ma and Zhong[4,5] and Zhong and Ma[6] refer to mode F as mode I and refer to mode S, not as a single family, but rather to the parts that comprise the family (Mack's first mode, second mode, etc.).

Mack used a nomenclature for these viscous families that was based on his inviscid nomenclature. However, at the time, the receptivity problem was not understood, and the decomposition of the solutions of the linearized Navier-Stokes equations had not been developed. We therefore suggest keeping the terminology corresponding to the normal mode analysis. The normal modes, mode S and mode F, are represented by separate poles in the complex plane, and they may be synchronized with slow and fast acoustic waves at a wave number $\alpha\to 0$.

IX. CONCLUSIONS

In this paper we solve the 3D initial-value problem for disturbances propagating in a compressible boundary layer in the parallel flow approximation. After resolving the issue with overlapping branch cuts, we showed that the solution can also be expressed as an expansion in a biorthogonal eigenfunction system. A numerical example that is used to investigate the spectrum of 3D disturbances in a 2D high-speed boundary layer flow leads to the following conclusions:

(1) Mode S and mode F are eigenvalue curves that correspond to separate solutions. Mathematically, each curve is the trajectory of a single pole in the complex p plane.
(2) Mode S contains regions of Mack first and second modes. Our results are consistent with Mack's[8,9] in so far as the mode S region comprised of Mack's second mode is most unstable to 2D disturbances, and the mode S region comprised of Mack's first mode is most unstable to a 3D disturbance.
(3) The discrete spectrum can change dramatically, depending on the angle of the disturbance propagation.
(4) Eigenvalue plots for choices of fixed spanwise wave number, β, show that the synchronism of mode S with the slow acoustic mode is primarily two-dimensional.
(5) At a sufficiently high angle of disturbance propagation, mode F ceases to synchronize with the entropy and vorticity modes.
(6) At a sufficiently high angle of disturbance propagation, the synchronism of mode S and mode F is no longer accompanied by a mode S instability. At even higher angles, there is no synchronism between mode S and mode F.

The synchronism observed in the example means that the phase velocities of the modes are the same. However, their complex eigenvalues are different. When the parallel flow assumption is used, as it has been for this analysis, the normal modes are orthogonal to one another and therefore do not interact with each other. However, this analysis may be extended to the case of nonparallel flow through the use of multiple scale methods. There will be a slow and a fast scale. At the level of the fast scale, the analysis shown here for parallel flow will be valid. At the level of the slow scale, the normal modes will interact and hence, one mode may be generated by another mode at the point of synchronism. Analysis of a nonparallel boundary layer flow was performed by Fedorov and Khokhlov[11] for the spatial stability problem. They showed that mode F may be generated by the vorticity/entropy modes. This decaying mode F may then effectively generate an unstable mode S. Additionally, this behavior has been seen in numerical studies for the spatial stability problem. Therefore, the features of the 3D spectrum found in our analysis of the initial-value problem might have a significant impact on the transition scenario in high-speed boundary layers. All the features discussed must be taken into account when designing transition experiments in hypersonic flows.

ACKNOWLEDGMENTS

The authors would like to thank Dr. Alexander Fedorov for his valuable comments. We would like to thank the National Science Foundation for providing a VIGRE graduate student fellowship to one of the authors. Additionally, this work was supported by the U.S. Air Force Office of Scientific Research. The authors benefited from the valuable comments and suggestions of anonymous reviewers.

APPENDIX: BIORTHOGONAL SYSTEM OF EIGENFUNCTIONS

It is possible to express a solution of the initial-value problem [Eq. (47)] as an expansion in the biorthogonal eigenfunction system $\{\mathbf{A}_\omega,\mathbf{B}_\omega\}$. The vector $\mathbf{A}_\omega$ is a solution of the direct problem

$$\frac{d}{dy}\left(\mathbf{L}_0\frac{d\mathbf{A}_\omega}{dy}\right)+\frac{d\mathbf{A}_\omega}{dy}=-i\omega\mathbf{H}_{10}\mathbf{A}_\omega+\mathbf{H}_{11}\mathbf{A}_\omega+i\alpha\mathbf{H}_2\mathbf{A}_\omega+i\alpha\mathbf{H}_3\frac{d\mathbf{A}_\omega}{dy}-\alpha^2\mathbf{H}_4\mathbf{A}_\omega+i\beta\mathbf{H}_5\mathbf{A}_\omega-\alpha\beta\mathbf{H}_6\mathbf{A}_\omega+i\beta\mathbf{H}_7\frac{d\mathbf{A}_\omega}{dy}-\beta^2\mathbf{H}_8\mathbf{A}_\omega, \tag{A1}$$

$$y=0:\quad \mathbf{A}_{\omega 1}=\mathbf{A}_{\omega 3}=\mathbf{A}_{\omega 5}=\mathbf{A}_{\omega 7}=0,$$

$$y\to\infty:\quad |\mathbf{A}_{\omega j}|<\infty\quad (j=1,\ldots,8). \tag{A2}$$

The vector $\mathbf{B}_\omega$ is a solution of the adjoint problem

$$\frac{d}{dy}\left(\mathbf{L}_0^*\frac{d\mathbf{B}_\omega}{dy}\right)-\frac{d\mathbf{B}_\omega}{dy}=i\bar{\omega}\mathbf{H}_{10}^*\mathbf{B}_\omega+\mathbf{H}_{11}^*\mathbf{B}_\omega-i\alpha\mathbf{H}_2^*\mathbf{B}_\omega+i\alpha\mathbf{H}_3^*\frac{d\mathbf{B}_\omega}{dy}-\alpha^2\mathbf{H}_4^*\mathbf{B}_\omega-i\beta\mathbf{H}_5^*\mathbf{B}_\omega-\alpha\beta\mathbf{H}_6^*\mathbf{B}_\omega+i\beta\mathbf{H}_7^*\frac{d\mathbf{B}_\omega}{dy}-\beta^2\mathbf{H}_8^*\mathbf{B}_\omega, \tag{A3}$$

$$y=0:\quad \mathbf{B}_{\omega 2}=\mathbf{B}_{\omega 4}=\mathbf{B}_{\omega 6}=\mathbf{B}_{\omega 8}=0,$$

$$y\to\infty:\quad |\mathbf{B}_{\omega j}|<\infty\quad (j=1,\ldots,8). \tag{A4}$$

The asterisk in Eq. (A3) denotes a Hermitian matrix, and the overbar denotes a complex conjugate value. The direct problem, Eqs. (A1) and (A2), can be expressed in the standard form given by Eq. (8). The adjoint problem, Eqs. (A3) and (A4), can be expressed in a similar fashion as

$$-\frac{d\mathbf{Y}}{dy}=\mathbf{H}_0^*\mathbf{Y}, \tag{A5}$$

$$y=0:\quad \mathbf{Y}_2=\mathbf{Y}_4=\mathbf{Y}_6=\mathbf{Y}_8=0,$$

$$y\to\infty:\quad |\mathbf{Y}_j|<\infty\quad (j=1,\ldots,8). \tag{A6}$$

A correspondence can be found between $\mathbf{B}_\omega$ and $\mathbf{Y}$. These relationships are given as follows:

$$B_1=Y_1+\frac{i\alpha rY_4}{[\mathrm{Re}/\mu_s-ir\gamma M_e^2(\alpha U_s+\beta W_s-\bar{\omega})]}, \tag{A7}$$

$$B_2=Y_2, \tag{A8}$$

$$B_3=i\alpha(m+1)Y_2+Y_3+\frac{rDT_s}{T_s}\frac{Y_4}{[\mathrm{Re}/\mu_s-ir\gamma M_e^2(\alpha U_s+\beta W_s-\bar{\omega})]}-\frac{r\mu_s}{\mathrm{Re}}\frac{d}{dy}\left(\frac{Y_4}{[1-ir\gamma M_e^2(\mu_s/\mathrm{Re})(\alpha U_s+\beta W_s-\bar{\omega})]}\right)+i\beta(m+1)Y_8, \tag{A9}$$

$$B_4=\frac{Y_4}{[1-ir\gamma M_e^2(\mu_s/\mathrm{Re})(\alpha U_s+\beta W_s-\bar{\omega})]}, \tag{A10}$$

$$B_5=Y_5-\frac{ir(\alpha U_s+\beta W_s-\bar{\omega})}{T_s}\times\frac{Y_4}{[\mathrm{Re}/\mu_s-ir\gamma M_e^2(\alpha U_s+\beta W_s-\bar{\omega})]}, \tag{A11}$$

$$B_6=Y_6, \tag{A12}$$

$$B_7=Y_7+i\beta r\frac{Y_4}{[\mathrm{Re}/\mu_s-ir\gamma M_e^2(\alpha U_s+\beta W_s-\bar{\omega})]}, \tag{A13}$$

$$B_8=Y_8. \tag{A14}$$

Solutions of the direct and adjoint problems given by Eqs. (A1), (A2), (A3), and (A4) belong to the discrete and continuous spectrum. Equations (32), (37), (39), (40), and (46) are modes that satisfy the direct problem with weights (coefficients) that depend on the Fourier transform of the initial disturbance, $\mathbf{A}_{0\alpha\beta}$.

The eigenfunction system $\{\mathbf{A}_\omega,\mathbf{B}_\omega\}$ has an orthogonality relation given as

$$\langle\mathbf{H}_{10}\mathbf{A}_\omega,\mathbf{B}_{\omega'}\rangle\equiv\int_0^\infty(\mathbf{H}_{10}\mathbf{A}_\omega,\mathbf{B}_{\omega'})dy=\Gamma\Delta_{\omega,\omega'}, \tag{A15}$$

where Γ is a normalization constant. $\Delta_{\omega,\omega'}$ is a Kronecker delta if either ω or ω' belong to the discrete spectrum. $\Delta_{\omega,\omega'}=\delta(\omega-\omega')$ is a Dirac delta function if both ω and ω' belong to the continuous spectrum.

The inverse Laplace transform can be expressed as an expansion in the biorthogonal eigenfunction system as follows:

$$\mathbf{A}_{\alpha\beta}(y,t)=\sum_\nu c_\nu\mathbf{A}_{\alpha\beta\omega_\nu}(y)e^{-i\omega_\nu t}+\sum_j\int_0^\infty c_j(k)\mathbf{A}_{\alpha\beta\omega_j}(y)e^{-iw_j(k)t}dk, \tag{A16}$$

where Σ_ν denotes a summation over the discrete spectrum and Σ_j denotes a summation over the continuous spectrum. Using the Fourier transform of the initial disturbance, $\mathbf{A}_{0\alpha\beta}$, as well as the orthogonality relation (Eq. (A15)), one can find the coefficients c_ν and c_j.

[1] E. Reshotko, "Boundary layer instability, transition and control," AIAA Paper No. 94-0001 (1994).
[2] G. B. Schubauer and H. K. Skramstad, "Laminar boundary-layer oscillations and stability of laminar flow," J. Aeronaut. Sci. **14**, 69 (1947).
[3] A. Fedorov and A. Tumin, "Initial-value problem for hypersonic boundary-layer flows," AIAA J. **41**, 379 (2003).
[4] Y. Ma and X. Zhong, "Receptivity of a supersonic boundary layer over a flat plate. Part 1. Wave structures and interactions," J. Fluid Mech. **488**, 31 (2003).
[5] Y. Ma and X. Zhong, "Receptivity of a supersonic boundary layer over a flat plate. Part 2. Receptivity to free-stream sound," J. Fluid Mech. **488**, 79 (2003).
[6] X. Zhong and Y. Ma, "Receptivity and linear stability of Stetson's mach 8 blunt cone stability experiments," AIAA Paper No. 2002-2849 (2002).
[7] L. H. Gustavsson, "Initial-value problem for boundary layer flows," Phys. Fluids **22**, 1602 (1979).
[8] L. M. Mack, "Boundary-layer stability theory," Jet Propulsion Lab., Report No. JPL 900-277, Pasadena, CA (1969).
[9] L. M. Mack, "Special course on stability and transition of laminar flow," AGARD Report 709 (1984).
[10] A. V. Fedorov, "Receptivity of a high-speed boundary layer to acoustic disturbances," J. Fluid Mech. **491**, 101 (2003).
[11] A. V. Fedorov and A. P. Khokhlov, "Prehistory of instability in a hypersonic boundary layer," Theor. Comput. Fluid Dyn. **14**, 359 (2001).
[12] See EPAPS Document No. E-PHFLE6-17-005509 for the nonzero elements of the matrices in Eqs. (2) and (8). This document can be reached via a direct link in the online article's HTML reference section or via the EPAPS homepage (http://www.aip.org/pubservs/epaps.html).

[13] J. D. Anderson, *Hypersonic and High Temperature Gas Dynamics* (AIAA, Reston, VA, 1989).
[14] M. R. Malik, "Numerical methods for hypersonic boundary layer stability," J. Comput. Phys. **86**, 376 (1990).
[15] H. Salwen and C. E. Grosch, "The continuous spectrum of the Orr-Sommerfeld equation. Part 2. Eigenfunction expansions," J. Fluid Mech. **104**, 445 (1981).
[16] V. R. Gushchin and A. V. Fedorov, "Asymptotic analysis of inviscid perturbations in a supersonic boundary layer," J. Appl. Mech. Tech. Phys. **30**, 64 (1989).